References and Notes

1. D. Schimel *et al.*, in *Climate Change 1995: The Science of Climate Change*, J. T. Houghton *et al.*, Eds. (Cambridge Univ. Press, Cambridge, 1996); R. J. Charlson, J. Langner, H. Rodhe, C. B. Leovy, S. G. Warren, *Tellus* **43AB**, 152 (1991).
2. E. P. Shettle and R. W. Fenn, *Technical Paper AFGL-TR-79-0214* (Air Force Geophysics Laboratory, Hanscom Air Force Base, Hanscom, MA, 1979); O. B. Toon and J. B. Pollack, *J. Appl. Meteorol.* **15**, 225 (1976).
3. J. Langner and H. Rodhe, *J. Atmos. Chem.* **13**, 225 (1991).
4. P. Kasibhatla, W. L. Chameides, J. St. John, *J. Geophys. Res.* **102**, 3737 (1997).
5. W. F. Cooke and J. J. N. Wilson, *ibid.* **101**, 19395 (1996).
6. C. Liousse *et al.*, *ibid.*, p. 19411.
7. I. Tegen and I. Fung, *ibid.* **100**, 18707 (1995).
8. I. Tegen *et al.*, *ibid.* **102**, 23895 (1997).
9. S. L. Gong *et al.*, *ibid.*, p. 3819.
10. J. A. Coakley, R. D. Cess, F. Yurevich, *J. Atmos. Sci.* **40**, 116 (1983).
11. E. F. Harrison *et al.*, *J. Geophys. Res.* **95**, 18687 (1990); V. Ramanathan *et al.*, *Science* **243**, 57 (1989).
12. J. M. Haywood and V. Ramaswamy, *J. Geophys. Res.* **103**, 6043 (1998).
13. F. J. Wentz, *IEEE Trans. Geosci. Remote Sensing* **30**, 960 (1997).
14. The radiation scheme used combines the delta-Eddington method with an exponential-sum fitting technique to handle multiple-scattering and molecular absorption (*12*). The parameterization has been developed and calibrated with high spectral resolution line-by-line adding-doubling solutions of Ramaswamy and Freidenreich [*J. Geophys. Res.* **103**, 23255 (1998)]. [See also S. M. Freidenreich and V. Ramaswamy, *Ninth Conference on Atmospheric Radiation*, Long Beach, CA, American Meteorological Society, February 1997, pp. 129–130; S. M. Freidenreich and V. Ramaswamy, in preparation.]
15. M. D. Glew, P. Hignett, J. P. Taylor, *J. Geophys. Res.*, in press.
16. The methodology of using the Geophysical Fluid Dynamics Laboratory (GFDL) Climate GCM for the particular set of experiments is similar to (*12*). The aerosol radiative effects do not feedback onto the GCM's dynamics. A single year is sufficient to accurately describe the annual clear-sky irradiances from the GCM because the sensitivity of the TOA irradiance to changes in meteorology (mainly water vapor concentrations) is small, and the prescribed ocean surface reflectance in the GCM does not have any interannual variation.
17. J. M. Haywood *et al.*, *J. Climatol.* **10**, 1562 (1997).
18. P. K. Quinn and D. J. Coffman, *J. Geophys. Res.*, in press.
19. "Low" sea-salt burdens are obtained with the formulation of R. F. Lovett [*Tellus* **30**, 358 (1978)]; "high" sea-salt burdens are obtained with the formulation of H. J. Exton *et al.* [in *Oceanic Whitecaps and Their Role in Air-Sea Exchange Processes*, E. C. Monahan and G. Mac Niocaill, Eds. (Reidel, Hingham, MA, 1986), pp. 195–208]. See also (*9*). The empirical formulations relate the sea-salt concentration (g/cm^3) to the local surface wind speed (m/s).
20. *WCP. A Preliminary Cloudless Standard Atmosphere for Radiation Computation* (World Meteorological Organization, Geneva, 1986).
21. O. B. Toon, J. B. Pollack, B. N. Khare, *J. Geophys. Res.* **81**, 5733 (1976).
22. I. Tegen, A. A. Lacis, I. Fung, *Nature* **380**, 419 (1996).
23. J. T. Kiehl and B. P. Briegleb, *Science* **260**, 311 (1993).
24. K. Taylor and J. E. Penner, *Nature* **369**, 734 (1994).
25. O. Boucher and T. L. Anderson, *J. Geophys. Res.* **100**, 26117 (1995).
26. From (*18*), the mean specific extinction at 70% relative humidity of the typically small and large particles constituting the sea-salt aerosol distribution is estimated as 8.7 and 1.9 m^2/g, respectively. The mass concentration in the supermicrometer mode is typically about 10 times (range 6 to 16 times) that in the submicrometer mode. Using the observations in (*18*), we estimate that the effective specific extinction for the entire distribution considering both the modes varies between 2.3 and 2.9 m^2/g. We adopted a value of 2.5 m^2/g and an asymmetry factor of 0.78 at 0.55 μm for the present calculations. Note that the value of the specific extinction is substantially greater than the one obtained by considering supermicrometer particles only (*18*).
27. The biases estimated for the clear-sky ERBE reflected solar irradiance fields are estimated to be about 1 W/m^2 or less when averaged over a 2.5° grid ocean box and over monthly-mean time scales; the monthly-mean results are estimated to have a root mean square bias of 2 W/m^2 or less (*11*). Bias estimates for zonal and global means are likely to be even smaller than for the regional means.
28. S. Cusack, A. Slingo, J. M. Edwards, M. Wild, *Q. J. R. Meterol. Soc.* **124**, 2181 (1998); J. T. Kiehl, J. J. Hack, J. W. Hurrell, *J. Climatol.* **11**, 1151 (1998).
29. As an indication of the sensitivity to uncertainties in water vapor, additional calculations for July 1988, with European Center for Medium Range Weather Forecasts (ECMWF) assimilated analyses of water vapor in place of the GCM water vapor fields, revealed differences of less than 20% from the biases shown in Fig. 1A.
30. Offline calculations performed with daily-mean rather than monthly-mean wind speeds yielded sea-salt concentrations that differ by ~15% on average. This difference is much smaller than the uncertainty in the mass-loading versus wind speed relation (*19*).
31. B. J. Soden and V. Ramaswamy, *Geophys. Res. Lett.* **25**, 2149 (1998).
32. D. M. Murphy *et al.*, *Nature* **392**, 62 (1998). Their measurements at a remote location indicate that much of the sulfur is on particles that also contain sea-salt. In effect, sea-salt aerosols provide reaction sites for the conversion of SO_2 to sulfate. The connection between sea-salt and sulfur cycles is also discussed by H. Sievering *et al.* [*ibid.* **360**, 571 (1992)] and N. A. Clegg and R. Toumi [*J. Geophys. Res.* **103**, 31095 (1998)]. Thus, for particles in the radiatively important size regime, the radiative contributions of sea-salt and sulfur may be linked. P. Quinn *et al.* [*ibid.*, p. 16547] point out that sea-salt controls the aerosol optical properties in the southern ocean in both the sub- and supermicrometer modes.
33. J. Latham and M. H. Smith, *Nature* **347**, 372 (1990).
34. The radiative effects of wind speed upon the sea-surface reflectance can be accounted for by including both a parameterization for the Fresnel effect [J. E. Hansen *et al.*, *Mon. Weather Rev.* **4**, 609 (1983)] and the effects of whitecaps [E. C. Monahan, *J. Phys. Oceanogr.* **1**, 139 (1971)]. Calculations performed with the assumption that the whitecaps are diffuse reflectors with an albedo of 0.6 suggest that the global surface reflectance is likely to decrease rather than increase as a function of wind speed; this cannot, therefore, explain the bias between model and observed reflected irradiances at the TOA seen in Fig. 1A.
35. We thank P. Kasibhatla and J. Langner for providing the sulfate climatologies, W. Cooke for providing the black carbon climatologies, I. Tegen for providing the dust climatologies, the NASA/Langley Distributed Active Archive Center (DAAC) for providing the ERBE data, the NASA/Jet Propulsion Laboratory DAAC for providing the SSMI data, and A. Broccoli, D. Schwarzkopf, R. Stouffer, and two anonymous reviewers for their comments and suggestions.

12 November 1998; accepted 26 January 1999

Lu-Hf Isotope Systematics of Garnet Pyroxenites from Beni Bousera, Morocco: Implications for Basalt Origin

Janne Blichert-Toft,[1]* Francis Albarède,[1] Jacques Kornprobst[2]

Six garnet pyroxenites from Beni Bousera, Morocco, yield a mean lutetium-hafnium age of 25 ± 1 million years ago and show a wide range in hafnium isotope compositions (ε_{Hf} = –9 to +42 25 million years ago), which exceeds that of known basalts (0 to +25). Therefore, primary melts of garnet pyroxenites cannot be the source of basalts. The upper mantle may be an aggregate of pyroxenites that were left by the melting of oceanic crust at subduction zones and peridotites that were contaminated by the percolation of melts from these pyroxenites. As a consequence, the concept of geochemical heterogeneities as passive tracers is inadequate. Measured lutetium-hafnium partitioning of natural minerals requires a reassessment of some experimental work relevant to mantle melting in the presence of garnet.

An upper mantle composition of depleted lherzolite with small zones of more mafic and fertile pyroxenite is consistent with the subduction of oceanic crust and the ubiquitous presence of pyroxenite layers in high-temperature peridotite massifs (*1*). The isotope geochemistry of Hf (*2*) and Th (*3*) seems to require the presence of residual garnet in the melting zone, even beneath the mid-ocean ridges (*4*). The compositional variability of oceanic basalts from mid-ocean ridge basalts (MORBs) to ocean island basalts could reflect either variable contributions of garnet pyroxenites to their source (*5–8*) or a broad pressure range of melting in a relatively homogeneous mantle (*9, 10*). The Nd-Hf isotopic properties of peridotite inclusions from the western United States have

---

[1] Ecole Normale Supérieure de Lyon and CNRS, 46 Allée d'Italie, 69364 Lyon Cedex 7, France. [2] L'Unité Mixte de Recherche CNRS "Magmas et Volcans," Observatoire de Physique du Globe de Clermont-Ferrand, 5 rue Kessler, 63038 Clermont-Ferrand, France.

*To whom correspondence should be addressed.

been found to be consistent with a zone of melting in the mantle that produces the Nd-Hf isotopic compositions measured in MORBs (*11*). By contrast, spinel-lherzolite samples from the suboceanic lithospheric mantle beneath Hawaii contain highly radiogenic Hf that has been interpreted as signaling metasomatic processes in the upper mantle (*11*). Our work complements these results with Lu-Hf isotope analyses of garnet pyroxenites and individual minerals from these rocks from high-temperature peridotite massifs. The rocks we focused on occur as layers (1 to 250 cm thick) that are intercalated (3 to 5% of the whole) within the mantle spinel-peridotites at Beni Bousera. Superimposed mineral assemblages in peridotites and in pyroxenites, from the diamond facies (*12*) down to the plagioclase-lherzolite facies, indicate that this piece of mantle experienced fast decompression and cooling before and during its hot emplacement within the granulitic metapelites (the so-called "kinzigites") of the lower continental crust, in which garnet pyroxenite intercalations also occur (*13, 14*). A geochemical comparison is introduced with eclogites from the ultramafic breccia that is associated with the metamorphic basal contact of the ophiolite pile of Mirdita, Albania (*15*), with the underlying country rocks.

Three of the clinopyroxene-garnet pairs and one whole-rock–garnet pair (sample M5-99), for which the Lu concentration of the clinopyroxene is not available, yield isochron ages of variable precision, although they are all consistent within error ranges (Table 1 and Fig. 1), with a weighted mean age of 25.0 ± 0.9 million years ago (Ma). Except for M5-99, where the whole-rock was included in the age calculation because of the lack of a complete Lu-Hf clinopyroxene analysis for this sample, whole rocks were excluded from age calculations on the grounds that they are more prone to grain boundary contamination by exotic phases. The Lu-Hf ages are older but not inconsistent with Sm-Nd clinopyroxene-garnet ages of 23.6 ± 4.3 Ma (Table 1, M5-101) and 23.0 ± 7.3 and 20.1 ± 6.9 Ma (*16*). The K-Ar and ^{39}Ar-^{40}Ar ages for mica and K feldspar of surrounding metapelites tend to cluster around 21 Ma (*17, 18*). Cooling from a temperature that is compatible with the blocking of cation exchange between garnet and clinopyroxene (>700°C) (*19*) [from a depth of at least 45 km (1.5 GPa) (*13*) and possibly from the diamond stability field at 150 km (5 GPa)] to a temperature of 300° to 400°C (at which mica and K feldspar start retaining Ar) should therefore have been taking place within 4 ± 2 million years. This supports a decompression rate of the rising peridotite on the order of 10 cm/year, which is indicative of a nearly adiabatic ascent and is consistent with the range of velocities associated with models of mantle convection and plate tectonics (*20*). Sample M5-15 gives an older Lu-Hf age of 66.4 ± 1.5 Ma, whereas the clinopyroxene-garnet pair from M6-214, emplaced into the surrounding kinzigites, gives an age of 30.6 ± 3 Ma. Such discrepancies may indicate that the Beni Bousera intrusion is a composite aggregate of rocks from different sources with a complicated ascent history that culminated at ~25 Ma.

The clinopyroxene-garnet age of sample K-398 from Mirdita, Albania, is 203.0 ± 3.4 Ma with the plotting of the whole-rock on the mineral isochron (Table 1 and Fig. 2). This age is older than the Sm-Nd age (166 ± 2 Ma) of the amphibole–clinopyroxene–garnet–whole-rock isochron reported for the same sample (*15*) and the ^{39}Ar-^{40}Ar age interval (163 to 174 Ma) for various amphibolites beneath the obduction thrust of Albanian ophiolites (*21*). Such a discordance may indicate that the garnet closure temperature to Lu and Hf diffusion is higher than that for Sm and Nd. The presence of amphibole in K-398 also suggests that the Mirdita garnet pyroxenite went through a stage of interaction with percolating fluids during the emplacement of the overlying ophiolite nappe that may have preferentially perturbed the Sm-Nd chronometric system, further contributing to its younger age.

Pyroxenites, viewed as a particularly fertile mantle component that could contribute to basalt genesis, have been associated so often with the chemical variability (*5*) and isotopic heterogeneities (*6*) of basalts that the concept of a mantle consisting of pyroxenite layers in a peridotite matrix ("marble cake") has become a popular paradigm of mantle geochemistry and basalt origin (*1*). The ^{176}Hf/^{177}Hf ratios of the whole-rock samples from the main intrusion of Beni Bousera at the time of emplacement [$\varepsilon_{\mathrm{Hf}}(T) = -9$ to $+42$] display a large isotopic range, from values that are less radiogenic than bulk silicate earth ($\varepsilon_{\mathrm{Hf}} = 0$ for all T) to values that are more radiogenic than any known modern oceanic basalt [$\varepsilon_{\mathrm{Hf}}(T) = 0$ to $+25$] (*22*). The least radiogenic Hf of the analyzed garnet pyroxenites is indistinguishable from that of the host kinzigite, which emphasizes that values typical of the continental crust may occur in ultramafic rocks. The variability of $\varepsilon_{\mathrm{Hf}}(T)$ of the Beni Bousera and Mirdita samples parallels the variability of Nd isotopes of Ronda and Beni Bousera samples (*16, 17, 23, 24*) with $\varepsilon_{\mathrm{Nd}}(T) = 0$ to $+26$. Such a heterogeneous signature rules out the possibility that the Beni Bousera intrusion represents a single piece of coherent oceanic lithosphere that was extracted from the asthenosphere within a short time interval. The Hf isotopic range of the garnet pyroxenites from Beni Bousera does not fit any known basaltic group, making this intrusion an unlikely potential source for mantle liquids.

The misfit between the Hf and Nd isotopic ranges of oceanic basalts and the garnet pyroxenites of this study cannot be reduced by subtracting the radiogenic growth within the

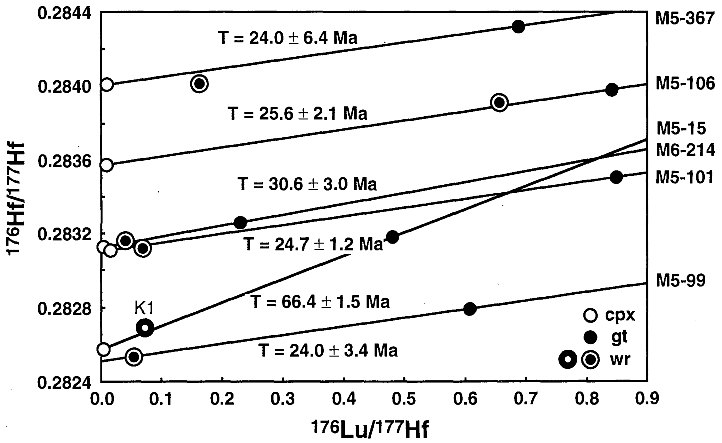

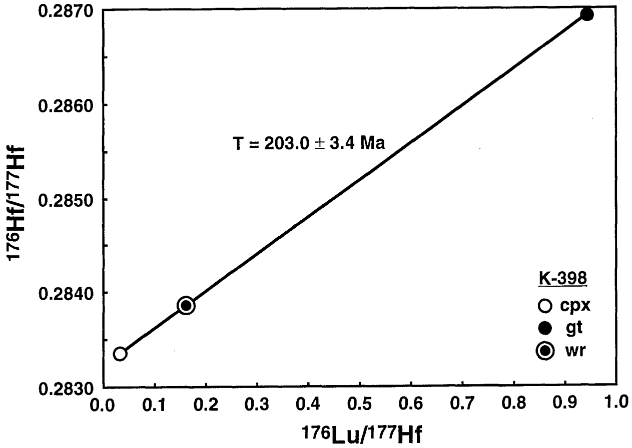

Fig. 1 (left). Lu-Hf isochron plot of five garnet pyroxenites from the Beni Bousera orogenic peridotite, Morocco. K1 is the host felsic granulite (kinzigite), and M6-214 is the associated garnet pyroxenite. Ages (T) refer to clinopyroxene-garnet pairs. Errors are propagated from the 2σ errors in Table 1. **Fig. 2 (right).** Lu-Hf isochron plot of one garnet pyroxenite from the ultramafic breccia beneath the Mirdita ophiolitic complex, Albania. The age refers to the clinopyroxene-garnet pair. Errors are as in Fig. 1.

rocks after crystallization. Even when whole-rock sample M5-106, whose mineralogy is biased by abundant garnet, is disregarded, the high $^{176}Lu/^{177}Hf$ ratios of the other samples indicate that parent/daughter fractionation occurred recently, possibly just before emplacement. The same conclusion holds true for the Sm-Nd data (*16*) and is also consistent with the recent age of cooling deduced from the coexistence of oxygen isotope heterogeneities over scales on the order of centimeters (*25*).

The Hf isotopic compositions of the garnet pyroxenites that we measured from Beni Bousera and Mirdita are inconsistent with a specific mantle component, such as EM I, EM II, or HIMU (*26*), that is identifiable in oceanic basalts. The $\delta^{18}O$ values (*25, 27*) signal that Beni Bousera garnet pyroxenites are not related to the source of MORBs. Their isotopically heavy oxygen ($\delta^{18}O > 6$) and radiogenic Os (*16*) are more reminiscent of the Koolau-type component that has been described for Hawaiian basalts and interpreted as reflecting the involvement of upper oceanic crust in the mantle source (*28*). By contrast, the low $\delta^{18}O$ value (+2.3) of Mirdita K-398 minerals may indicate recycling of the deeper parts of oceanic crust (*15*).

The whole-rock Lu/Hf ratios of the present samples, which are all superchondritic, mirror the depletion of light rare-earth elements in pyroxenite (*29*) and suggest that these rocks represent either cumulates or residues from melting events in the presence of garnet. Pearson *et al.* (*25*) argued that the large range of Ni and Cr contents of these rocks requires mineral accumulation in magma conduits and that their high $\delta^{18}O$ values point to the source of these magmas as having been exposed to low-temperature interaction with seawater or hydrothermal fluids. Difficulties associated with this model are given as follows: (i) basalts that have high $\delta^{18}O$ values are uncommon; (ii) for a strong Ni enrichment in the cumulate, more olivine than that present in pyroxenites is required, implying that contents high in Ni must be inherited from parent melts; and (iii) the brittle regime required by magma conduit injection contrasts with the high temperature and pressure conditions of mineral equilibration at Beni Bousera (*13*).

We propose, in agreement with previous suggestions (*1, 29*), that pyroxenites primarily represent residues that were left by the melting of subducted oceanic crust and that these residues were subsequently refolded plastically with the enclosing peridotite. The oceanic precursors, which were fractionated at low pressure, should be dominated by olivine or plagioclase, which, upon melting, would give rise to Ni- and Al-rich garnet pyroxenites, respectively [the latter being characterized by positive Eu anomalies (*30*)]. The Hf isotope systematics and the sharp $\delta^{18}O$ transition between pyroxenite layers and ambient peridotite indicate that the refolding and melting events (and associated Lu/Hf and Sm/Nd fractionation) would have to have been recent and might have coincided with the nearly adiabatic ascent that occurred just before emplacement.

In addition, some type of open system behavior with metasomatic transport is needed to account for the presence of radiogenic Hf in peridotite xenoliths from Salt Lake crater, Hawaii, with no corresponding excess radiogenic Nd (*11*). Although the garnet pyroxenites, which are similar to those investigated in our work, are residual, they can still produce melts at temperatures ~100°C below the peridotite solidus (*31*). These melts would have high Lu/Hf ratios and would preserve the anomalous $\delta^{18}O$ of their oceanic crust protolith. Because they are undersaturated in olivine, the melts are expected to react with the ambient mantle peridotite and to produce, over short distances, a broad variety of metasomatized peridotites (*32*)

Table 1. Lu-Hf and Sm-Nd isotope data for six garnet pyroxenites and the host felsic granulite (kinzigite) from the Beni Bousera orogenic peridotite, Morocco, and one garnet pyroxenite from the Mirdita ophiolite complex, Albania. Lu-Hf chemistry and isotope measurements were carried out as described in (*34*) using steel-jacketed teflon bombs for sample dissolution. The uncertainties reported on Hf and Nd measured isotope ratios are $2\sigma/\sqrt{n}$ analytical errors in the last decimal place; *n* is the number of measured isotopic ratios; ppm, parts per million; gt, garnet; cpx, clinopyroxene; wr, whole-rock. Dashes indicate data not available.

Sample	[Lu]* (ppm)	[Hf]† (ppm)	$^{176}Lu/^{177}Hf$*	$^{176}Hf/^{177}Hf$‡	$\varepsilon_{Hf}(T)$§	[Sm]† (ppm)	[Nd]† (ppm)	$^{147}Sm/^{144}Nd$†	$^{143}Nd/^{144}Nd$‖	$\varepsilon_{Nd}(T)$§
Beni Bousera orogenic peridotite										
M5-15 gt	1.15	0.341	0.4800	0.283187 ± 10	+7.1	–	–	–	–	–
M5-15 cpx	0.0698	3.03	0.0033	0.282576 ± 7	−6.4	–	–	–	–	–
M5-99 wr	0.179	0.472	0.0539	0.282537 ± 14	−8.7	–	–	–	–	–
M5-99 wr	0.185	0.468	0.0561	0.282596 ± 10	−6.6	–	–	–	–	–
M5-99 gt	0.687	0.161	0.6078	0.282794 ± 33	−9.0	–	–	–	–	–
M5-99 cpx	–	1.16	–	0.282594 ± 49	–	–	–	–	–	–
M5-99 cpx	–	–	–	0.282595 ± 45	–	–	–	–	–	–
M5-101 wr	0.498	1.04	0.0681	0.283120 ± 10	+11.7	1.25	3.05	0.2467	0.513029 ± 9	+7.5
M5-101 gt	1.61	0.268	0.8492	0.283505 ± 14	+12.0	0.34	0.12	1.7371	0.513255 ± 37	+7.1
M5-101 cpx	0.0947	0.875	0.0154	0.283107 ± 13	+12.2	0.62	1.02	0.3686	0.513044 ± 12	+7.4
M5-106 wr	1.38	0.299	0.6559	0.283912 ± 27	+29.7	–	–	–	–	–
M5-106 gt	1.35	0.228	0.8407	0.283983 ± 19	+29.1	–	–	–	–	–
M5-106 cpx	0.0483	0.861	0.0080	0.283571 ± 27	+28.7	–	–	–	–	–
M5-367 wr	0.669	0.592	0.1605	0.284014 ± 5	+41.8	–	–	–	–	–
M5-367 wr	0.666	0.591	0.1600	0.283978 ± 17	+40.5	–	–	–	–	–
M5-367 gt	0.908	0.188	0.6864	0.284322 ± 81	+43.7	–	–	–	–	–
M5-367 cpx	0.106	1.45	0.0103	0.284009 ± 18	+44.1	–	–	–	–	–
M6-214 wr	0.469	1.69	0.0393	0.283159 ± 4	+13.6	2.58	5.73	0.2722	0.513043 ± 14	+7.7
M6-214 gt	0.974	0.604	0.2289	0.283257 ± 11	+13.8	2.22	1.42	0.9458	0.513023 ± 157	+5.1
M6-214 cpx	0.0631	2.42	0.0037	0.283124 ± 10	+13.0	3.05	8.29	0.2221	0.513051 ± 10	+8.0
M6-214 cpx	0.0707	2.50	0.0040	0.283122 ± 28	+12.9	–	–	–	–	–
K1 (kinzigite) wr	0.600	1.19	0.0715	0.282690 ± 6	−3.6	–	–	–	–	–
Mirdita ophiolite complex¶										
K-398 wr	0.291	0.256	0.1614	0.283830 ± 13	+19.6	0.64	1.04	0.3742	0.513224 ± 27	+6.8
K-398 gt	1.05	0.158	0.9444	0.286925 ± 13	+20.4	0.49	0.23	1.2705	0.514200 ± 95	+2.6
K-398 cpx	0.0888	0.395	0.0319	0.283366 ± 45	+21.2	0.98	1.76	0.3358	0.513211 ± 14	+7.6

*2σ errors for Lu concentration and for $^{176}Lu/^{177}Hf$ are <1.0%. †2σ errors for Sm, Nd, and Hf concentrations and for $^{147}Sm/^{144}Nd$ are <0.5%. ‡Normalized for mass fractionation to $^{179}Hf/^{177}Hf = 0.7325$. $^{176}Hf/^{177}Hf$ of JMC-475 Hf standard = 0.28216 ± 1. §ε_{Hf} and ε_{Nd} values were calculated at 25 Ma for Beni Bousera and at 203 Ma for Mirdita with $^{176}Hf/^{177}Hf_{CHUR(0)} = 0.282772$ and $^{176}Lu/^{177}Hf_{CHUR(0)} = 0.0332$ and with $^{143}Nd/^{144}Nd_{CHUR(0)} = 0.512638$ and $^{147}Sm/^{144}Nd_{CHUR(0)} = 0.1967$, respectively. ‖Normalized for mass fractionation to $^{146}Nd/^{144}Nd = 0.7219$. $^{143}Nd/^{144}Nd$ of La Jolla Nd standard = 0.511826 ± 13 (M5-101 and M6-214) and 0.511835 ± 10 (K-398). ¶Sm and Nd isotope data are from (*15*).

before freezing on their way to the surface. The symmetrical mineralogical layering of the pyroxenite layers, which has been taken as indicating a magmatic fractionation sequence (*25*), is also consistent with melt-mediated mineral reactions at length scales of tens of centimeters. For small fractions of melt, the oxygen isotope composition of the peridotite would be preserved, but the Hf isotopic signature would not. It would instead be dominated by the radiogenic melt component. The extreme Nd and Hf isotopic properties of many peridotites and pyroxenites require that truly primary melts never get sampled as basalts.

The solution to the origin-of-basalt dilemma (*10, 31*), which suggests either isobaric melting of a heterogeneous pyroxenite/peridotite source or polybaric melting of a more homogeneous peridotite source, may rather be a combination of these two scenarios. A "normal" piece of mantle may be dominated by coexisting pyroxenite residues and peridotites that were contaminated by the pervasive circulation of pyroxenite melts. Although the "marble cake" mantle is a seminal concept, the present isotopic evidence suggests that the original ingredients became somewhat mixed up, or even preferentially lost, to the point that the original recipe has become difficult to decipher. Geochemical heterogeneities therefore should be handled as active rather than as passive Lagrangian tracers by convection models.

The lower Lu/Hf ratio of oceanic basalts with respect to the time-integrated ratio deduced for the mantle source of the basalts from their Hf isotope systematics is an apparent inconsistency (dubbed the "Hf paradox"), which Salters and Hart (*2*) explained by the presence of garnet during melting. This model has recently been challenged by Blundy *et al.* (*4*), who redetermined the partition coefficients of clinopyroxene and melt and found that, at 1.5 GPa and for small degrees of melting (1%), Lu, Hf, Sm, and Nd are five times more compatible than currently thought. They combined these data with results on garnet (*33*) to create a critical partitioning parameter (CPP) $(D_{\mathrm{Sm}}/D_{\mathrm{Nd}})/(D_{\mathrm{Lu}}/D_{\mathrm{Hf}})$, where D stands for the mineral/melt partition coefficients, which they use to argue that the Nd-Hf isotope systematics of MORBs do not require residual garnet during melting. Although garnet pyroxenites cannot be used to infer the CPP of each mineral, ratios of CPP for garnet and clinopyroxene at mantle conditions may be inferred from mineral/mineral partitioning, provided that subsolidus reequilibration is not extreme. In our samples, which were equilibrated at pressures of at least 1.5 GPa (*13*), which is close to the experimental conditions of Blundy *et al.* (*4*), the Lu/Hf fractionation between garnet (ga) and clinopyroxene (cpx) is strong with $(D_{\mathrm{Lu}}/D_{\mathrm{Hf}})_{\mathrm{ga}}/(D_{\mathrm{Lu}}/D_{\mathrm{Hf}})_{\mathrm{cpx}}$ in the range of 55 to 150. These values can be combined with the $(D_{\mathrm{Sm}}/D_{\mathrm{Nd}})_{\mathrm{ga}}/(D_{\mathrm{Sm}}/D_{\mathrm{Nd}})_{\mathrm{cpx}}$ value of ~5, which was observed in our study and in (*16*), to produce a $\mathrm{CPP}_{\mathrm{ga}}/\mathrm{CPP}_{\mathrm{cpx}}$ ratio that is in the range of 0.03 to 0.1, which is well below the range of 0.8 to 2.1 deduced from the experimental data (*4, 33*). Part of the reason for this inconsistency may be that the experimental partition coefficients have not been obtained on a molten assemblage with garnet and clinopyroxene coexisting in the residue. We nevertheless consider that the compatibility of Sm, Nd, Lu, and Hf in clinopyroxene may have been overestimated by previous experiments and that residual garnet in the source of basalts still represents the best answer to the Hf paradox.

References and Notes

1. C. J. Allègre and D. L. Turcotte, *Nature* **323**, 123 (1986).
2. V. J. M. Salters and S. R. Hart, *ibid.* **342**, 420 (1989).
3. T. Z. LaTourrette, A. K. Kennedy, G. J. Wasserburg, *Science* **261**, 739 (1993).
4. J. D. Blundy, J. A. C. Robinson, B. J. Wood, *Earth Planet. Sci. Lett.* **160**, 493 (1998).
5. D. A. Wood, *Geology* **7**, 499 (1979).
6. A. Zindler, H. Staudigel, R. Batiza, *Earth Planet. Sci. Lett.* **70**, 175 (1984).
7. M. Roy-Barman and C. J. Allègre, *ibid.* **129**, 145 (1995).
8. C. C. Lundstrom, Q. Williams, J. B. Gill, *ibid.* **157**, 151 (1998).
9. D. McKenzie and R. K. O'Nions, *J. Petrol.* **32**, 1021 (1991).
10. B. Bourdon, A. Zindler, T. Elliott, C. H. Langmuir, *Nature* **384**, 231 (1996).
11. V. J. M. Salters and A. Zindler, *Earth Planet. Sci. Lett.* **129**, 13 (1995).
12. V. V. Slodkevitch, *Mineral. Soc. U.S.S.R.* **1**, 13 (1982).
13. J. Kornprobst, *Contrib. Mineral. Petrol.* **23**, 283 (1969).
14. ______, *Notes Serv. Geol. Maroc* **251**, 1 (1974).
15. K. Gjata, J. Kornprobst, A. Kodra, D. Briot, F. Pineau, *Bull. Soc. Geol. Fr.* **163**, 469 (1992).
16. N. Kumar, L. Reisberg, A. Zindler, *Geochim. Cosmochim. Acta* **60**, 1429 (1996).
17. D. G. Pearson, G. R. Davies, P. H. Nixon, *J. Petrol.* **34**, 125 (1993).
18. T. P. Loomis, *Am. J. Sci.* **275**, 1 (1975).
19. S. Duchêne *et al.*, *Nature* **387**, 586 (1997).
20. Y. Ricard and C. Vigny, *J. Geophys. Res.* **94**, 17543 (1989).
21. P. Vergely, A. Dimo, P. Monié, *C. R. Acad. Sci. Paris* **326**, 717 (1998).
22. References for Hf isotope data in oceanic basalts can be obtained from J. Blichert-Toft upon request.
23. L. Reisberg and A. Zindler, *Earth Planet. Sci. Lett.* **81**, 29 (1986/1987).
24. ______, E. Jagoutz, *ibid.* **96**, 161 (1989).
25. D. G. Pearson, G. R. Davies, P. H. Nixon, P. B. Greenwood, D. P. Mattey, *ibid.* **102**, 289 (1991).
26. A. Zindler and S. Hart, *Annu. Rev. Earth Planet. Sci.* **14**, 493 (1986).
27. M. Javoy, in *Orogenic Mafic and Ultramafic Association*, vol. 272 of *Colloques Internationaux du CNRS*, C. J. Allègre and J. Aubouin, Eds. (Editions du CNRS, Paris, 1980), pp. 279–287.
28. J. C. Lassiter, E. H. Hauri, P. W. Reiners, M. O. Garcia, *Mineral. Mag.* **62A**, 856 (1998).
29. M. Loubet and C. J. Allègre, *Nature* **298**, 809 (1982).
30. J. Kornprobst, M. Piboule, M. Roden, A. Tabit, *J. Petrol.* **31**, 717 (1990).
31. M. M. Hirschmann and E. M. Stolper, *Contrib. Mineral. Petrol.* **124**, 185 (1996).
32. E. H. Hauri, *Earth Planet. Sci. Lett.* **153**, 1 (1997).
33. W. van Westrenen, J. Blundy, B. Wood, *Am. Mineral.*, in press.
34. J. Blichert-Toft, C. Chauvel, F. Albarède, *Contrib. Mineral. Petrol.* **127**, 248 (1997).

35. We are grateful to P. Télouk for keeping the Plasma 54 inductively coupled plasma mass spectrometer in optimum working condition. We thank two anonymous reviewers for helpful comments.

22 October 1998; accepted 20 January 1999

Seismic Evidence for a Detached Indian Lithospheric Mantle Beneath Tibet

G. Kosarev,[1] R. Kind,[2,3]* S. V. Sobolev,[2] X. Yuan,[2]
W. Hanka,[2] S. Oreshin[1]

P-to-S converted teleseismic waves recorded by temporary broadband networks across Tibet show a north-dipping interface that begins 50 kilometers north of the Zangbo suture at the depth of the Moho (80 kilometers) and extends to a depth of 200 kilometers beneath the Bangong suture. Under northern Tibet a segmented south-dipping structure was imaged. These observations suggest a different form of detachment of the Indian and Asian lithospheric mantles caused by differences in their composition and buoyancy.

Although the altitude of the Tibetan Plateau is uniform, physical properties of the lithosphere (crust and upper mantle) such as velocity and density are different in northern and southern Tibet (*1–16*), suggesting fundamental differences in the origin of the lithosphere in these two regions. In the upper mantle in northern Tibet, the propagation of S_n waves is inefficient (*8, 9*), P_n velocities are slow (*5*), and there exists a low-velocity body (*16*). Together with evidence for a higher Poisson ratio in the crust of northern Tibet (*2*) and the presence of volcanic activity (*17*), these data suggest

---

[1] Institute of the Physics of the Earth, Russian Academy of Sciences, B. Gruzinskaya 10, 128810 Moscow, Russia. [2] GeoForschungsZentrum Potsdam, Telegrafenberg, 14473 Potsdam, Germany. [3] Freie Universität Berlin, Geophysik, Malteser Strasse 74-100, 12249 Berlin, Germany.

*To whom correspondence should be addressed. E-mail: kind@gfz-potsdam.de